

Higher-order topological phases emerging from the Su-Schrieffer-Heeger stacking

Xun-Jiang Luo,^{1,2} Xiao-Hong Pan,^{1,2} Chao-Xing Liu,³ and Xin Liu^{1,2,*}

¹*School of Physics and Institute for Quantum Science and Engineering, Huazhong University of Science and Technology, Wuhan, Hubei 430074, China*

²*Wuhan National High Magnetic Field Center and Hubei Key Laboratory of Gravitation and Quantum Physics, Wuhan, Hubei 430074, China*

³*Department of Physics, the Pennsylvania State University, University Park, PA, 16802, US*

In this work, we develop a systematical approach of constructing and classifying the model Hamiltonians for two-dimensional (2D) higher-order topological phase with corner zero energy states (CZESs). Our approach is based on the direct construction of analytical solution of the CZESs in a series of 2D systems that stack the 1D extended Su-Schrieffer-Heeger (SSH) model, two copies of the original SSH model, along two orthogonal directions. Fascinatingly, our approach not only gives the celebrated Benalcazar-Bernevig-Hughes and 2D SSH models but also reveals a novel model and we refer it to crossed 2D SSH model. Although these three models exhibit completely different bulk topology, we find that the CZESs can be universally characterized by edge winding number for 1D edge states, attributing to their unified Hamiltonian construction form and edge topology. Remarkably, our principle of obtaining CZESs can be readily generalized to arbitrary dimension and superconducting systems. Thus, our work sheds new light on the theoretical understanding of the higher-order topological phase and paves the way to looking for higher-order topological insulators and superconductors.

Introduction - Over the past few years, the concept of topological phases has been generalized to higher-order [1–4], which has been extensively studied in electronic [5–8], bosonic [9–15], Floquet [16–20], non-Hermitian [21–25] and quasicrystal systems [26–30]. Especially in condensed matter system, the higher-order topological insulators [31–35] and superconductors [36–40], featuring corner or hinge states, have been attracting increasing attentions. Generally speaking, the corner states of higher-order topological phase with additional chiral or particle-hole symmetry, will appear at the center of their energy spectrum, namely zero energy. Particularly in the superconducting system with intrinsic particle-hole symmetry, the exact zero energy corner states, dubbed as Majorana corner states, follow non-Abelian braiding statistics and allow the implementation of topological quantum computation [41]. Recently, it has been shown that the corner zero energy states (CZESs) in electronic system also present nontrivial braiding properties [42].

The CZE have been studied in various higher-order topological systems [43–55]. However, the established topological invariants characterization of CZESs is usually case by case. For example, the well-known Benalcazar-Bernevig-Hughes (BBH) [1] and 2D SSH models [56] are two paradigms featuring the CZE, which are characterized by the quantized quadruple moment [57, 58] and bulk polarization [56], respectively. Although exhibiting different topological characterization, the BBH and 2D SSH models are both constructed from stacking the extended SSH models, two copies of the original SSH model [59]. This motivates us to systematically investigate the 2D systems of stacking the 1D extended SSH models along different directions. For these systems, two open questions are urgent to be answered. Firstly,

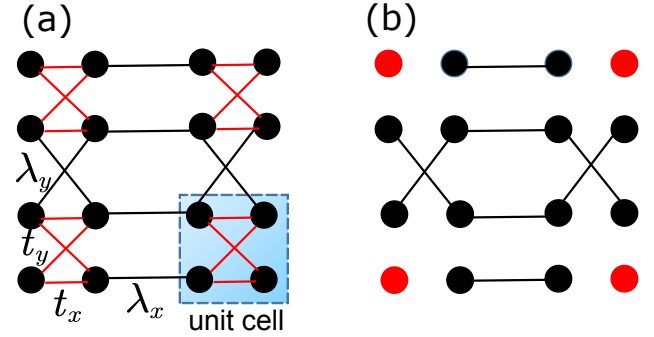


FIG. 1. Schematic diagram for the lattice hoppings of crossed 2D SSH model. (a) Red and black bonds represent the intra-cellular and inter-cellular hoppings, respectively. (b) The limit case $t_{x,y} = 0$ in (a).

do these systems always support the CZESs? Secondly, are there general topological characterizations for the obtained CZESs?

In this work, we establish a general analytical theory to provide the CZESs existing condition in the systems, stacking the 1D extended SSH model along two orthogonal directions. This condition not only naturally presents the BBH and 2D SSH models, but also leads to a novel model displaying second-order topology. We can visually distinguish this new model from the BBH and 2D SSH models by its crossed hoppings along y-direction (Fig.1(a)). We thus call it crossed 2D SSH model. Although exhibiting completely different bulk topology, we find that the CZESs in the BBH, 2D SSH and 2D crossed SSH models can be uniformly characterized by the edge winding number for 1D edge states, which elucidates the unified edge-corner correspondence [60–62]. Moreover,

Our theory can be easily generalized to 3D systems and predicts the mass of 3D higher-order topological phases.

Constructing corner zero energy states- Generally, we consider the 2D model Hamiltonian written as

$$H(\mathbf{k}) = \sum_{s=x,y} h_s(k_s),$$

$$h_s(k_s) = M_s(k_s)\Gamma_s^a + \lambda_s \sin k_s \Gamma_s^b, \quad (1)$$

where $M_s(k_s)$ is defined as $t_s + \lambda_s \cos k_s$ and $\Gamma_s^{a(b)}$, belonging to 15 traceless 4×4 Dirac matrices, satisfy the anti-commutation relation $\{\Gamma_s^a, \Gamma_s^b\} = 0$. Consequently, each 1D Hamiltonian h_s respects chiral symmetry $C_s = i\Gamma_s^a \Gamma_s^b$, with $C_s^2 = 1$. As each Dirac matrix has two-fold degenerate eigenvalue, the three Dirac matrices $\{\Gamma_s^a, \Gamma_s^b, C_s\}$ form the reducible representation of SU(2) Lie algebra: $h_s(k_s)$ can be considered as the direct sum of two copies of SSH model. Accordingly, the topology of h_s is determined by the winding number ν_s of the vector $(M_s, \lambda_s \sin k_s)$ around origin point [66]. Then the topologically nontrivial phase is constrained in the region $|t_s| < |\lambda_s|$, corresponding to $\nu_s = 1$. Taking $s = x$ for example, each end exists two end zero states in topologically nontrivial region and their wave functions can be obtained by solving the equation [66]

$$h_x(x)|\Psi(x)\rangle = 0, \quad (2)$$

with $h_x(x)$ the real space Hamiltonian. We find that the end zero states are the eigenstates of C_x with eigenvalue z_x , and the end states labelled by $z_x = -1$ and $z_x = 1$ are localized at left and right ends, respectively. Consequently, the 1D end zero states wave function can be generically written as

$$|\Psi_{z_x}(x)\rangle = f_{z_x}(x)|\psi_{z_x}\rangle. \quad (3)$$

where $f_{-(+)}(x)$ is the spatial wave function localized at left (right) end and the spinor $|\psi_{z_x}\rangle$ satisfies $C_x|\psi_{z_x}\rangle = z_x|\psi_{z_x}\rangle$.

Similarly, for the 1D Hamiltonian h_y , we have

$$h_y(y)|\Psi_{z_y}(y)\rangle = 0,$$

$$|\Psi_{z_y}(y)\rangle = g_{z_y}(y)|\psi_{z_y}(y)\rangle, \quad (4)$$

To understand above solution visually, the end zero states of h_x and h_y are schematically denoted by the color balls in Figs. 2(a) and (b). However, we note that only the nontrivial topology of both h_x and h_y can not guarantee the existence of CZESs for 2D Hamiltonian H . This can be best exemplified by the well-known Bernevig-Hughes-Zhang model [67, 68], in which the nontrivial topology of h_x and h_y give gapless edge states but without corner states. Remarkably, we find that the CZEs can be obtained when additional general condition, namely $[C_x, C_y]_- = 0$ is satisfied. Under this condition, operators C_x and C_y have four common eigenstates $|\psi_{(z_x, z_y)}\rangle$, labelled by their eigenvalues (z_x, z_y) ,

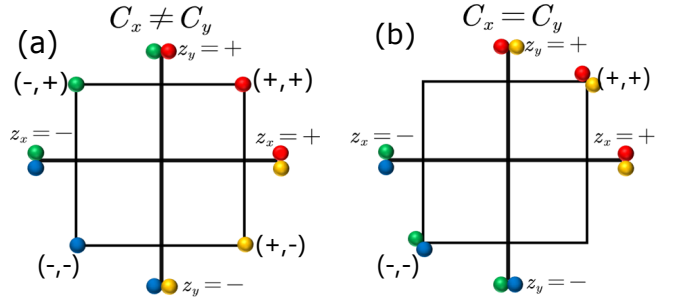


FIG. 2. (a)(b) Schematic diagram of the end zero states and CZESs spatial distribution under different situations. The black square frame denotes the boundary of the 2D system described by Hamiltonian $H(\mathbf{k})$. The horizontal and perpendicular lines correspond to the 1D systems described by Hamiltonians h_x and h_y , respectively. The four-color balls are the four common eigenstates of operators C_x and C_y , denoting the end zero states or CZESs, labelled by eigenvalues (z_x, z_y) . The relation between the end zero states and CZESs can be guided by the color of the balls.

with $(z_x, z_y) \in \{(+, +), (+, -), (-, +), (-, -)\}$. Then we can construct the 2D wave function

$$|\Psi_{(z_x, z_y)}(\mathbf{r})\rangle = f_{z_x}(x)g_{z_y}(y)|\psi_{(z_x, z_y)}\rangle. \quad (5)$$

It is easy to see that

$$h_x(x)|\Psi_{(z_x, z_y)}(\mathbf{r})\rangle = 0, h_y(y)|\Psi_{(z_x, z_y)}(\mathbf{r})\rangle = 0, \quad (6)$$

resulting in $H(\mathbf{r})|\Psi_{(z_x, z_y)}(\mathbf{r})\rangle = 0$. Obviously, the state $|\Psi_{(z_x, z_y)}(\mathbf{r})\rangle$ exponentially decays along both x, y directions, which indicates that it is a CZES for the 2D system. Thus, we can conclude that $H(\mathbf{r})$ hosts four CZESs when $\nu_x, \nu_y = 1$ and $[C_x, C_y]_- = 0$.

Classification- Explicitly, the condition $[C_x, C_y]_- = 0$ can be divided into two situations, namely (a): $C_x \neq C_y$ and (b): $C_x = C_y$. Here, we do not distinguish the equivalent cases $C_x = C_y$ and $C_x = -C_y$. For situation (a), the four common eigenstates are labeled by $(z_x, z_y) = \{(+, +), (+, -), (-, +), (-, -)\}$. Thus, the corresponding four CZESs, schematically distinguished by the red, yellow, green and blue balls in Fig. 2(a), are localized at each corner according to Eq. 5. For situation (b), because of $z_x = z_y$, the four common eigenstates of C_x and C_y are labeled by $(z_x, z_y) = \{(+, +), (+, +), (-, -), (-, -)\}$. As a result, the four corresponding CZESs are localized at the diagonal corners, shown in Fig. 2(b). Notably, up to now our analysis is general and the specific form of $H(\mathbf{k})$ has not been given. However, the topological property of $H(\mathbf{k})$ deeply depend on the given form. In the following, we perform classification of $H(\mathbf{k})$ under the condition $[C_x, C_y] = 0$.

As any two Dirac matrices either commute or anti-commute to each other, the second-order topological phase described by $H(k)$ can be further classified by the commutation relations between $\Gamma_x^{a,b}$ and $\Gamma_y^{a,b}$ under the

condition $[C_x, C_y] = 0$, or equivalently $[i\Gamma_x^a \Gamma_x^b, i\Gamma_y^a \Gamma_y^b] = 0$. It is straightforwardly to show that there exist four inequivalent cases with the commutation relations

$$\begin{aligned}
 \text{(i)} : & \{\Gamma_x^a, \Gamma_y^{a,b}\} = 0, \{\Gamma_x^b, \Gamma_y^{a,b}\} = 0; \\
 \text{(ii)} : & [\Gamma_x^a, \Gamma_y^{a,b}] = 0, [\Gamma_x^b, \Gamma_y^{a,b}] = 0; \\
 \text{(iii)} : & [\Gamma_x^a, \Gamma_y^{a,b}] = 0, \{\Gamma_x^b, \Gamma_y^{a,b}\} = 0; \\
 \text{(iv)} : & [\Gamma_x^a, \Gamma_y^a] = 0, \{\Gamma_x^b, \Gamma_y^b\} = 0 \\
 & \{\Gamma_x^a, \Gamma_y^b\} = 0, [\Gamma_x^b, \Gamma_y^b] = 0
 \end{aligned} \quad (7)$$

Considering concrete representation of the Dirac matrices, we find that situations $C_x \neq C_y$ and $C_x = C_y$ correspond to the cases (i-iv) and (iv), respectively [66]. On the other hand, it can be readily verified that $H(\mathbf{k})$ has bulk chiral symmetry \mathcal{C} with $\{\mathcal{C}, H(\mathbf{k})\} = 0$ for all the cases. Concretely, $\mathcal{C} = C_x C_y$ and $\mathcal{C} = C_x$ for cases (i-ii) and cases (iii-iv), respectively. Since the CZESs are labelled by eigenvalues (z_x, z_y) , the CZE is the eigenstate of \mathcal{C} , with eigenvalue $z = z_x z_y$ or $z = z_x$. With this property, the CZESs labelled by the same eigenvalue of operator \mathcal{C} can not be coupled by the perturbations preserving the bulk chiral symmetry [69], which allows a Z topological classification for the CZESs of second-order topological insulator phase.

In case (i), matrices $\{\Gamma_x^{a,b}, \Gamma_y^{a,b}\}$ anti-commute with each other, corresponding to the BBH model. In case (ii), h_x and h_y commute with each other, corresponding to the 2D SSH model. Remarkably, the commutation relations in the (iii) and (iv) predict two unprecedented models. Case (iii) corresponds to the crossed 2D SSH model (Fig. 1). In case (iv), we find that the CZESs always coexist with the edge flat band [66], which brings the difficulty to identify and characterize the CZESs. In the following, we focus on the crossed 2D SSH model.

Crossed 2D SSH model- Considering the concrete representation of the Dirac matrices, the Hamiltonian for case (iii) can be written as

$$\begin{aligned}
 \mathcal{H}(\mathbf{k}) &= h_x(k_x) + h_y(k_y), \\
 h_x(k_x) &= M_x(k_x)\tau_x\sigma_0 + \lambda_x \sin k_x \tau_y \sigma_0, \\
 h_y(k_y) &= M_y(k_y)\tau_x\sigma_x + \lambda_y \sin k_y \tau_x \sigma_y,
 \end{aligned} \quad (8)$$

with τ, σ two sets of Pauli matrices. The corresponding lattice hopping of $\mathcal{H}(\mathbf{k})$ is schematically shown in Fig. 1(a), which has dimerized hopping in x -direction as the 1D SSH model and crossed hopping in y -direction. Therefore, we refer to this model as the crossed 2D SSH model. In Fig. 1(b), the isolated atoms at the corner in the limit case $t_{x,y} = 0$ correspond to the CZESs.

To study the bulk phase and band structures of $\mathcal{H}(\mathbf{k})$, we simplify $\mathcal{H}(\mathbf{k})$ as

$$\mathcal{H}(\mathbf{k}) = M_x(k_x)\tau_x\sigma_0 + \lambda_x \sin k_x \tau_y \sigma_0 + E_y \tau_x \sigma_\varphi, \quad (9)$$

with $\sigma_\varphi = \cos \varphi \sigma_x + \sin \varphi \sigma_y$, $\cos \varphi = M_y/E_y$, $E_y = \sqrt{M_y^2 + (\lambda_y \sin k_y)^2}$. In the eigenbasis of σ_φ ($\sigma_\varphi = \pm 1$),

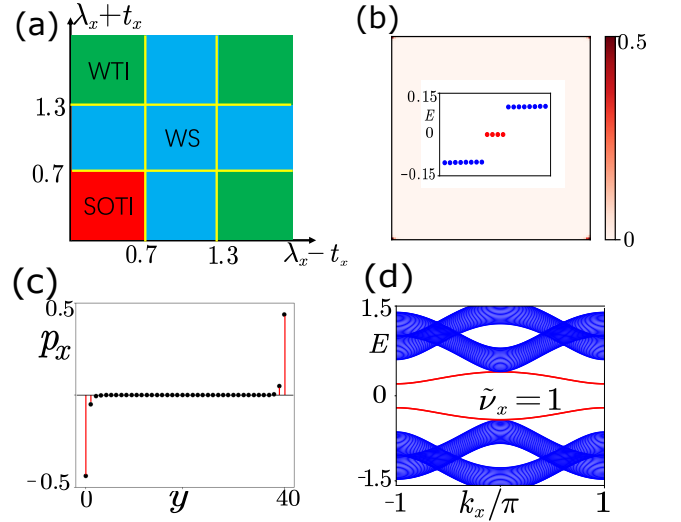


FIG. 3. (a) The phase diagram of the second-order topological phase in 2D crossed model. The bulk phase transitions, represented by the yellow line, divide the bulk states into weak topological insulator (WTI), Weyl semimetal (WS), or second-order topological insulator (SOTI) phases. (b) Spatial distribution of the CZESs in the 2D crossed SSH model, the inset plots the eigenenergies close to zero. (c) Numerical calculation of edge polarization p_x . (d) Energy dispersion of nanoribbon structure along y direction. The red bands denote the edge states. Common parameters in (a)(c)(d) are taken with $t_x = 0.1$, $\lambda_x = 0.2$, $t_y = 0.3$, $\lambda_y = 1$.

$\mathcal{H}(\mathbf{k})$ is block-diagonal and the two blocks Hamiltonian can be written as

$$h_{\pm}(\mathbf{k}) = (M_x \pm E_y)\tau_x + \lambda_x \sin k_x \tau_y, \quad (10)$$

with \pm corresponding to the eigenvalues of σ_φ . As a result, we can reveal the 2D bulk spectrum of $\mathcal{H}(\mathbf{k})$ in Eq. (9) through the spectrum of $h_{\pm}(\mathbf{k})$, which can be considered as the 1D SSH model along k_x -direction with k_y -dependent hopping amplitude $t_x \pm E_y$. Given k_y , the topology of 1D SSH Hamiltonians $h_{\pm}(\mathbf{k})$ is characterized by the quantized Berry phase $\alpha_{\pm}(k_y)$ of occupied states. We classify the bulk states of Eq. (9) into three phases based on the first-order topological band theory: when $\alpha_+(k_y)$ and $\alpha_-(k_y)$ are both quantized to π over all the range of k_y , the SSH models in Eq. (10) are fully gapped so that the bulk energy spectrum of $\mathcal{H}(\mathbf{k})$ in Eq. (9) is also fully gapped. The system can be viewed as the pile-up of 1D topologically non-trivial SSH model, which is weak topological insulator with flat edge band [66]; when $\alpha_+(k_y)$ and $\alpha_-(k_y)$ are both quantized to 0 over all the range of k_y , the SSH models in Eq. (10) and the bulk energy spectrum of $\mathcal{H}(\mathbf{k})$ in Eq. (9) are also fully gapped. The system is a trivial insulator; when $\alpha_+(k_y)$ or $\alpha_-(k_y)$ has a transition with varying k_y , the SSH models in Eq. (10) and the bulk energy spectrum of $\mathcal{H}(\mathbf{k})$ in Eq. (9) close their gaps at certain k_y along high symmetry line $k_x = 0$ or π . The system be-

TABLE I. Topological characterization of the CZESs by various topological invariants. Here, $\tilde{\nu}$ denotes the edge winding number of 1D edge states along x -direction.

invariant Case	$(p_x^{\nu_y}, p_y^{\nu_x})$	(P_x, P_y)	Q_{xy}	$\tilde{\nu}_x$
(i)(BBH)	✓	×	✓	✓
(ii)(2D SSH)	×	✓	×	✓
(iii)	×	×	✓	✓

comes mirror symmetry ($\mathcal{M}_x = \tau_x \sigma_0$) protected Weyl semimetal [66, 70]. Having clarified the bulk phase, we plot the bulk phase diagram in Fig. 3(a) under the parameters $\lambda_y = 1, t_y = 0.3$ and $0 < t_x < \lambda_x$. In this CZESs existing parameters region, we find that the bulk states can be divided into second-order topological insulator (the CZESs shown in Fig. 3(b)), weak topological insulator and Weyl semimetal through the creation or annihilation of the Weyl points, represented by the yellow line in Fig. 3(a). The absence of bulk-corner correspondence implies that the CZESs may not origin from the bulk topology.

On the other hand, for characterizing the CZESs, several bulk topological invariants have been established, including nested Wilson loop $(p_x^{\nu_y}, p_y^{\nu_x})$ [1, 2], bulk polarization (P_x, P_y) [56, 71], quadrupole moment Q_{xy} [57, 58]. Here, we test the applicability of characterizing the 2D crossed SSH model by these topological invariants and take the BBH and 2D SSH models as comparison. We find that the nested Wilson loop and polarization topological characterizations only apply to BBH and 2D SSH model, respectively [66]. Moreover, the quadrupole moment topological characterization apply to both BBH and crossed 2D SSH models [66]. However distinct from the BBH model with edge polarization [1, 2] $p_x^{\text{edge}} = p_y^{\text{edge}} = 0.5$, the crossed 2D SSH model exhibits nontrivial edge polarization only along x -direction [66] and $p_x^{\text{edge}} = 0.5$ is shown in Fig. 3(c). Thus, the crossed 2D SSH model provides a paradigm of type-II quadrupole topological insulator [72], featuring nonzero quadrupole moment and one direction edge polarization. Although absence of unified characterization by these bulk topological invariants, we find that the CZESs in BBH, 2D SSH and 2D crossed SSH models can be uniformly characterized by nonzero winding number for 1D edge states [66]. We take the crossed 2D SSH model for example following.

Note that the in gap edge state (red curves in Fig. 3(d)), corresponding to the edge-localized states, extend over the whole 1D Brillouin zone. Thus, these edge states can be described by truly 1D lattice Hamiltonian, which is essential to define edge winding number for 1D edge states unambiguously. Directly, the wave function of the edge states can be obtained by solving the equation $\mathcal{H}(k_x, y)|\Psi(k_x, y)\rangle = E(k_x)|\Psi(k_x, y)\rangle$. Because of $[h_x, C_y]_- = 0$, the edge state $\Psi(k_x, y)\rangle$ are the common

eigenstate of C_y and h_x , showing as

$$\begin{aligned} |\Psi(k_x, y)\rangle &= g_+(y)P|\Phi(k_x)\rangle, \\ h_x(k_x)|\Phi(k_x)\rangle &= E_x(k_x)|\Phi(k_x)\rangle, \end{aligned} \quad (11)$$

with $E_x(k_x) = \sqrt{M_x^2 + (\lambda_x \sin k_x)^2}$ and the edge projection operator $P = (1 + C_y)/2$ [73, 74]. The edge Hamiltonian can be obtained by projecting h_x to the subspace defined by P , leading to the edge Hamiltonian

$$\tilde{h}_x(k_x) = M_x(k_x)\tilde{\tau}_x + \lambda_x \sin k_x \tilde{\tau}_y. \quad (12)$$

with $\tilde{\tau}$ acting the subspace where $C_y = 1$. Obviously, $\tilde{h}_x(k_x)$ behaves as the SSH model and is topologically nontrivial when $\nu_x = 1$. On the other hand, the existence of edge states depend on the condition that h_y is topologically nontrivial, namely $\nu_y = 1$. Thus, the edge winding number $\tilde{\nu}_x = 1$ defined by the occupied states of \tilde{h}_x can precisely characterize the CZESs existing condition $\nu_{x,y} = 1$. Remarkably, the commutation relation $[h_x, C_y] = 0$ is the main reason for the existence of well defined winding number of 1D edge states. It can be readily that $[h_x, C_y] = 0$ also holds in the BBH and 2D SSH model according to Eq. (7). Thus, the edge winding number characterization also applies to the BBH and 2D SSH models owing to the unified commutation relation $[h_x, C_y] = 0$, which also reflects the CZESs existing condition $[C_x, C_y] = 0$.

Higher dimensional generalizations- Our principle of constructing the CZESs can be easily generalized to arbitrary dimension [66]. Here, we consider 3D eight bands Hamiltonian

$$\begin{aligned} H(\mathbf{k}) &= \sum_{s=x,y,z} h_s(k_s), \\ h_s(k) &= (t_s + \lambda_s \cos k_s)\Gamma_{as}^8 + \lambda_s \sin k_s \Gamma_{bs}^8, \end{aligned} \quad (13)$$

where 8×8 Gamma matrices $\Gamma_{as,bs}^8$ [66] anti-commute with each other and the chiral symmetry of h_s is given by $C_s = i\Gamma_{as}^8 \Gamma_{bs}^8$. Similarly, h_s can be deemed as the direct sum of four copies of SSH model and then h_s exists four end zero states at each end. Remarkably, when 8×8 matrices $\{C_x, C_y, C_z\}$ commute with each other, they have eight common eigenstates. Correspondingly, eight CZESs of 3D Hamiltonian H can be constructed according our general principle. However, to determine the topological property of $H(\mathbf{k})$, we need to specify the commutation relations between all the Gamma matrices. On the other hand, our 2D classification indicates that there are four types commutation relations between matrices $\{\Gamma_{as}^8, \Gamma_{bs}^8, \Gamma_{as'}^8, \Gamma_{bs'}^8\}$ under the condition $[C_s, C_{s'}]_- = 0$, where $\{s, s'\} \in \{x, y\}, \{x, z\}, \{y, z\}$. Thus, classifying $H(\mathbf{k})$ can predict 64 models featuring CZESs when do not distinguish the equivalent status between different directions. A typical example is the topological octupole insulator model [1, 2, 75], in which all the Gamma matrices anti-commute with each other. We study other predicted models featuring the CZESs in our future work.

Discussion and Conclusion—It is noted that our theory of obtaining the CZESs can readily be generalized to the superconducting system by requiring an additional particle-hole symmetry. Some higher-order topological superconductors can be predicted [66]. In view of the experiment realization of the BBH and 2D SSH models [10–12, 76–80], we believe that the crossed 2D SSH model can also be realized in various artificial lattice systems. It is also worth emphasizing that our theory of obtaining the CZESs can be easily generalized to obtain the hinge states with analytical solutions. Thus in our theoretical framework, we can systematically construct arbitrary order topological insulators and superconductors in arbitrary dimension by directly constructing the analytical solution of boundary states, which is left as an independent work.

In summary, we provide a general analytical theory to study the higher-order topological phase emerging from SSH stacking. Our theory not only gives the well-known BBH and 2D SSH models, but also predicts the crossed 2D SSH model. We establish the unified topological characterizing of these three models. Our work provides a broad venue to looking for higher-order topological phases in arbitrary dimension.

* phyliuxin@hust.edu.cn

- [1] W. A. Benalcazar, B. A. Bernevig, and T. L. Hughes, *Science* **357**, 61 (2017).
- [2] W. A. Benalcazar, B. A. Bernevig, and T. L. Hughes, *Phys. Rev. B* **96**, 245115 (2017).
- [3] Z. Song, Z. Fang, and C. Fang, *Phys. Rev. Lett.* **119**, 246402 (2017).
- [4] J. Langbehn, Y. Peng, L. Trifunovic, F. von Oppen, and P. W. Brouwer, *Phys. Rev. Lett.* **119**, 246401 (2017).
- [5] F. Schindler, A. M. Cook, M. G. Vergniory, Z. Wang, S. S. P. Parkin, B. A. Bernevig, and T. Neupert, *Science Advances* **4**, 0346 (2018).
- [6] M. Geier, L. Trifunovic, M. Hoskam, and P. W. Brouwer, *Phys. Rev. B* **97**, 205135 (2018).
- [7] F. Schindler, Z. Wang, M. G. Vergniory, A. M. Cook, A. Murani, S. Sengupta, A. Y. Kasumov, R. Deblock, S. Jeon, I. Drozdov, H. Bouchiat, S. Guéron, A. Yazdani, B. A. Bernevig, and T. Neupert, *Nature Physics* **14**, 918 (2018).
- [8] E. Khalaf, *Phys. Rev. B* **97**, 205136 (2018).
- [9] B.-Y. Xie, H.-F. Wang, H.-X. Wang, X.-Y. Zhu, J.-H. Jiang, M.-H. Lu, and Y.-F. Chen, *Phys. Rev. B* **98**, 205147 (2018).
- [10] M. Serra-Garcia, V. Peri, R. Süssstrunk, O. R. Bilal, T. Larsen, L. G. Villanueva, and S. D. Huber, *Nature* **555**, 342 (2018).
- [11] B.-Y. Xie, G.-X. Su, H.-F. Wang, H. Su, X.-P. Shen, P. Zhan, M.-H. Lu, Z.-L. Wang, and Y.-F. Chen, *Phys. Rev. Lett.* **122**, 233903 (2019).
- [12] X.-D. Chen, W.-M. Deng, F.-L. Shi, F.-L. Zhao, M. Chen, and J.-W. Dong, *Phys. Rev. Lett.* **122**, 233902 (2019).
- [13] X. Ni, M. Weiner, A. Alù, and A. B. Khanikaev, *Nature Materials* **18**, 113 (2019).
- [14] H. Fan, B. Xia, L. Tong, S. Zheng, and D. Yu, *Phys. Rev. Lett.* **122**, 204301 (2019).
- [15] H. Xue, Y. Yang, G. Liu, F. Gao, Y. Chong, and B. Zhang, *Phys. Rev. Lett.* **122**, 244301 (2019).
- [16] M. Rodriguez-Vega, A. Kumar, and B. Seradjeh, *Phys. Rev. B* **100**, 085138 (2019).
- [17] Y. Peng and G. Refael, *Phys. Rev. Lett.* **123**, 016806 (2019).
- [18] Y. Peng, *Phys. Rev. Research* **2**, 013124 (2020).
- [19] H. Hu, B. Huang, E. Zhao, and W. V. Liu, *Phys. Rev. Lett.* **124**, 057001 (2020).
- [20] B. Huang and W. V. Liu, *Phys. Rev. Lett.* **124**, 216601 (2020).
- [21] T. Liu, Y.-R. Zhang, Q. Ai, Z. Gong, K. Kawabata, M. Ueda, and F. Nori, *Phys. Rev. Lett.* **122**, 076801 (2019).
- [22] Z. Zhang, M. Rosendo López, Y. Cheng, X. Liu, and J. Christensen, *Phys. Rev. Lett.* **122**, 195501 (2019).
- [23] X.-W. Luo and C. Zhang, *Phys. Rev. Lett.* **123**, 073601 (2019).
- [24] E. Edvardsson, F. K. Kunst, and E. J. Bergholtz, *Phys. Rev. B* **99**, 081302 (2019).
- [25] K. Kawabata, M. Sato, and K. Shiozaki, *Phys. Rev. B* **102**, 205118 (2020).
- [26] D. Varjas, A. Lau, K. Pöyhönen, A. R. Akhmerov, D. I. Pikulin, and I. C. Fulga, *Phys. Rev. Lett.* **123**, 196401 (2019).
- [27] R. Chen, C.-Z. Chen, J.-H. Gao, B. Zhou, and D.-H. Xu, *Phys. Rev. Lett.* **124**, 036803 (2020).
- [28] C.-B. Hua, R. Chen, B. Zhou, and D.-H. Xu, *Phys. Rev. B* **102**, 241102 (2020).
- [29] S. Spurrier and N. R. Cooper, *Phys. Rev. Research* **2**, 033071 (2020).
- [30] B. Lv, R. Chen, R. Li, C. Guan, B. Zhou, G. Dong, C. Zhao, Y. Li, Y. Wang, H. Tao, J. Shi, and D.-H. Xu, *Communications Physics* **4**, 108 (2021).
- [31] K. Wang, J.-X. Dai, L. B. Shao, S. A. Yang, and Y. X. Zhao, *Phys. Rev. Lett.* **125**, 126403 (2020).
- [32] C.-A. Li, B. Fu, Z.-A. Hu, J. Li, and S.-Q. Shen, *Phys. Rev. Lett.* **125**, 166801 (2020).
- [33] B. Liu, L. Xian, H. Mu, G. Zhao, Z. Liu, A. Rubio, and Z. F. Wang, *Phys. Rev. Lett.* **126**, 066401 (2021).
- [34] C.-A. Li, S.-B. Zhang, J. Li, and B. Trauzettel, *Phys. Rev. Lett.* **127**, 026803 (2021).
- [35] P.-L. Zhao, X.-B. Qiang, H.-Z. Lu, and X. C. Xie, *Phys. Rev. Lett.* **127**, 176601 (2021).
- [36] Y.-T. Hsu, W. S. Cole, R.-X. Zhang, and J. D. Sau, *Phys. Rev. Lett.* **125**, 097001 (2020).
- [37] M. Kheirikhah, Z. Yan, Y. Nagai, and F. Marsiglio, *Phys. Rev. Lett.* **125**, 017001 (2020).
- [38] R.-X. Zhang and S. Das Sarma, *Phys. Rev. Lett.* **126**, 137001 (2021).
- [39] X.-J. Luo, X.-H. Pan, and X. Liu, *Phys. Rev. B* **104**, 104510 (2021).
- [40] A. K. Ghosh, T. Nag, and A. Saha, *Phys. Rev. B* **104**, 134508 (2021).
- [41] C. Nayak, S. H. Simon, A. Stern, M. Freedman, and S. Das Sarma, *Rev. Mod. Phys.* **80**, 1083 (2008).
- [42] Y. Wu, H. Jiang, J. Liu, H. Liu, and X. C. Xie, *Phys. Rev. Lett.* **125**, 036801 (2020).
- [43] Z. Yan, F. Song, and Z. Wang, *Phys. Rev. Lett.* **121**, 096803 (2018).

- [44] C.-H. Hsu, P. Stano, J. Klinovaja, and D. Loss, Phys. Rev. Lett. **121**, 196801 (2018).
- [45] Q. Wang, C.-C. Liu, Y.-M. Lu, and F. Zhang, Phys. Rev. Lett. **121**, 186801 (2018).
- [46] X.-L. Sheng, C. Chen, H. Liu, Z. Chen, Z.-M. Yu, Y. X. Zhao, and S. A. Yang, Phys. Rev. Lett. **123**, 256402 (2019).
- [47] X.-H. Pan, K.-J. Yang, L. Chen, G. Xu, C.-X. Liu, and X. Liu, Phys. Rev. Lett. **123**, 156801 (2019).
- [48] X. Zhu, Phys. Rev. Lett. **122**, 236401 (2019).
- [49] Y. Volpez, D. Loss, and J. Klinovaja, Phys. Rev. Lett. **122**, 126402 (2019).
- [50] R.-X. Zhang, W. S. Cole, and S. Das Sarma, Phys. Rev. Lett. **122**, 187001 (2019).
- [51] Y. Ren, Z. Qiao, and Q. Niu, Phys. Rev. Lett. **124**, 166804 (2020).
- [52] Y.-J. Wu, J. Hou, Y.-M. Li, X.-W. Luo, X. Shi, and C. Zhang, Phys. Rev. Lett. **124**, 227001 (2020).
- [53] X. Wu, W. A. Benalcazar, Y. Li, R. Thomale, C.-X. Liu, and J. Hu, Phys. Rev. X **10**, 041014 (2020).
- [54] C. Chen, Z. Song, J.-Z. Zhao, Z. Chen, Z.-M. Yu, X.-L. Sheng, and S. A. Yang, Phys. Rev. Lett. **125**, 056402 (2020).
- [55] L. Chen, B. Liu, G. Xu, and X. Liu, Phys. Rev. Research **3**, 023166 (2021).
- [56] F. Liu and K. Wakabayashi, Phys. Rev. Lett. **118**, 076803 (2017).
- [57] B. Kang, K. Shiozaki, and G. Y. Cho, Phys. Rev. B **100**, 245134 (2019).
- [58] W. A. Wheeler, L. K. Wagner, and T. L. Hughes, Phys. Rev. B **100**, 245135 (2019).
- [59] W. P. Su, J. R. Schrieffer, and A. J. Heeger, Phys. Rev. Lett. **42**, 1698 (1979).
- [60] M. Ezawa, Phys. Rev. B **102**, 121405 (2020).
- [61] L. Trifunovic, Phys. Rev. Research **2**, 043012 (2020).
- [62] Y.-S. Hu, Y.-R. Ding, J. Zhang, Z.-Q. Zhang, and C.-Z. Chen, Phys. Rev. B **104**, 094201 (2021).
- [63] A. P. Schnyder, S. Ryu, A. Furusaki, and A. W. W. Ludwig, Phys. Rev. B **78**, 195125 (2008).
- [64] S. Ryu, A. P. Schnyder, A. Furusaki, and A. W. W. Ludwig, New Journal of Physics **12**, 065010 (2010).
- [65] C.-K. Chiu, J. C. Y. Teo, A. P. Schnyder, and S. Ryu, Rev. Mod. Phys. **88**, 035005 (2016).
- [66] See appendixes for a detailed description of the Dirac matrices and their generalization, wave function of the end zero states, the general construction of CZESs, the details and comparisons of different cases in 2D system, the CZSSs in the superconducting system.
- [67] B. A. Bernevig, T. L. Hughes, and S.-C. Zhang, Science **314**, 1757 (2006).
- [68] The well-known BHZ model can be separated into the form written as a summation of two SSH models along different directions, with $\Gamma_x^a = \Gamma_y^a$. However, this system does not exist the CZSSs in real space.
- [69] If the perturbation h_p preserves the chiral symmetry \mathcal{C} , with $[h_p, \mathcal{C}]_+ = 0$. Then the coupling between the CZSSs with same eigenvalue z can be expressed as $\langle \Psi_z | h_p | \Psi_z \rangle = z \langle \Psi_z | (\mathcal{C} h_p + h_p \mathcal{C}) / 2 | \Psi_z \rangle = 0$.
- [70] Because the two bands which cross to form the Wely nodes have opposite eigenvalue of mirror-x symmetry $\mathcal{M}_x = \tau_x \sigma_0$, the perturbations preserving the mirror symmetry can not remove the Wely nodes.
- [71] W. A. Benalcazar, T. Li, and T. L. Hughes, Phys. Rev. B **99**, 245151 (2019).
- [72] Y.-B. Yang, K. Li, L.-M. Duan, and Y. Xu, Phys. Rev. Research **2**, 033029 (2020).
- [73] E. Khalaf, H. C. Po, A. Vishwanath, and H. Watanabe, Phys. Rev. X **8**, 031070 (2018).
- [74] E. Roberts, J. Behrends, and B. Béri, Phys. Rev. B **101**, 155133 (2020).
- [75] J. Bao, D. Zou, W. Zhang, W. He, H. Sun, and X. Zhang, Phys. Rev. B **100**, 201406 (2019).
- [76] M. Serra-Garcia, R. Süssstrunk, and S. D. Huber, Phys. Rev. B **99**, 020304 (2019).
- [77] S. Imhof, C. Berger, F. Bayer, J. Brehm, L. W. Molenkamp, T. Kiessling, F. Schindler, C. H. Lee, M. Greiter, T. Neupert, and R. Thomale, Nature Physics **14**, 925 (2018).
- [78] S. Mittal, V. V. Orre, G. Zhu, M. A. Gorlach, A. Poddubny, and M. Hafezi, Nature Photonics **13**, 692 (2019).
- [79] L.-Y. Zheng, V. Achilleos, O. Richoux, G. Theocharis, and V. Pagneux, Phys. Rev. Applied **12**, 034014 (2019).
- [80] Y. Qi, C. Qiu, M. Xiao, H. He, M. Ke, and Z. Liu, Phys. Rev. Lett. **124**, 206601 (2020).
- [81] Y. Wang, M. Lin, and T. L. Hughes, Phys. Rev. B **98**, 165144 (2018).
- [82] A. Tiwari, A. Jahin, and Y. Wang, Phys. Rev. Research **2**, 043300 (2020).

Supplemental Materials

Dirac matrices and their generalization

Starting from three anti-commuting Pauli matrices $\sigma_{x,y,z}$ and 2×2 identity matrix σ_0 , the 16 Dirac matrices $\sigma_i \otimes \sigma_j (\sigma_i \sigma_j)$ can be obtained through their direct product, with $i = j = x, y, z, 0$. Besides 4×4 identity matrix, the other 15 Dirac matrices are traceless and they square to identify. For the 15 traceless Dirac matrices, the five of them anti-commuting with each other. Without loss of generality, we can choose the five anti-commuting matrices as

$$\Gamma_1^4 = \sigma_z \sigma_x, \Gamma_2^4 = \sigma_z \sigma_y, \Gamma_3^4 = \sigma_z \sigma_z, \Gamma_4^4 = \sigma_x \sigma_0, \Gamma_5^4 = \sigma_y \sigma_0. \quad (14)$$

Other 10 traceless Dirac matrices can be generated by $\Gamma_{mn}^4 = \frac{1}{2i}[\Gamma_m^4, \Gamma_n^4]$, with $m = n = 1, 2, 3, 4, 5$. Generalizing to higher dimension, the direct product of arbitrary d sets Pauli matrices can generate 4^d Gamma matrices $\sigma_i \cdots \sigma_j \cdots \sigma_k$ with dimension 2^d and they square to identify. In these 4^d Gamma matrices, $2d + 1$ matrices anti-commuting with each other, forming complex Clifford algebra. Generally, the $2d + 1$ anti-commuting matrices can be obtained through the iteration from $2d - 1$ anti-commuting Gamma matrices with dimension $2^{d-1} \times 2^{d-1}$

$$\Gamma_{1,2,\dots,2d-1}^{2^d} = \sigma_z \otimes \Gamma_{1,2,\dots,2d-1}^{2^{d-1}}, \Gamma_{2d}^{2^d} = \sigma_x \otimes I^{2^{d-1}}, \Gamma_{2d+1}^{2^d} = \sigma_y \otimes I^{2^{d-1}}, \quad (15)$$

where $I^{2^{d-1}}$ denotes the $2^{d-1} \times 2^{d-1}$ identity matrix, $\Gamma_{1,2,\dots,2d-1}^{2^{d-1}}$ represents $2d - 1$ anti-commuting Gamma matrices with dimension $2^{d-1} \times 2^{d-1}$.

1D extended SSH model

In the momentum space, we consider the general model Hamiltonian in AIII symmetry class[63–65].

$$h(k) = M(k)\Gamma_a^{2^d} + \lambda \sin k \Gamma_b^{2^d}, \quad (16)$$

where $M(k) = (t + \lambda \cos k)$, $\Gamma_{a,b}^{2^d}$ are $2^d \times 2^d$ Gamma matrices and satisfy $\{\Gamma_a^{2^d}, \Gamma_b^{2^d}\} = 0$. The chiral symmetry of h can be written as $C = i\Gamma_a^{2^d}\Gamma_b^{2^d}$. It is noted that $h(k)$ is block-diagonal in certain basis and each 2×2 block Hamiltonian behave as the SSH model. Thus, $h(k)$ can be generically deemed as the direct sum of 2^{d-1} copies of SSH model. In the following, we characterize the topology of $h(k)$ by topological invariant winding number.

The energy spectrum of h is $E = \sqrt{(t + \lambda \cos k)^2 + (\lambda \sin k)^2}$. For simplicity, h can be normalized as

$$\bar{h} = \cos \varphi \Gamma_a^{2^d} + \sin \varphi \Gamma_b^{2^d}, \quad (17)$$

with $\cos \varphi = (t + \lambda \cos k)/E$. With the dimension and symmetry class given, the topology of \bar{h} is determined by the winding number

$$\bar{\nu} = -\frac{1}{4i\pi} \int_{-\pi}^{\pi} \text{Tr}[C \bar{h} d\bar{h}] \quad (18)$$

$$= -\frac{1}{4i\pi} \int_{-\pi}^{\pi} \text{Tr}[(\cos \varphi \partial_k \cos \varphi + \sin \varphi \partial_k \sin \varphi)C + (\cos \varphi \partial_k \sin \varphi - \sin \varphi \partial_k \cos \varphi)C \Gamma_a^{2^d} \Gamma_b^{2^d}] \quad (19)$$

$$= \frac{2^d}{4\pi} \int_{-\pi}^{\pi} (\cos \varphi \partial_k \sin \varphi - \sin \varphi \partial_k \cos \varphi) \quad (20)$$

$$= \frac{2^d}{4\pi} \int_{-\pi}^{\pi} \partial_k \varphi. \quad (21)$$

In the parameter region $|t| < |\lambda|$, above integration yields topological invariant $\bar{\nu} = 2^{d-1}$. Otherwise, $\bar{\nu} = 0$. Owing to the bulk-boundary correspondence, the winding number $\bar{\nu}$ is associated with 2^{d-1} end zero states localized at each end under the open boundary condition. In the following, we solve the analytical wave function of these end zero states.

Considering the semi-infinite system ($r > 0$) described by h , we solve the end zero states localized close to the end $r = 0$. Directly, we expand the Hamiltonian h at $k = 0$ to second order of k and replace $k \rightarrow -i\partial_r$. Then we have

$$h(-i\partial_r) = (m + \lambda/2\partial_r^2)\Gamma_a^{2^d} - i\lambda\partial_r\Gamma_b^{2^d}, \quad (22)$$

with $m = t + \lambda$. Solving the eigen equation $h(-i\partial_r)|\Phi_\alpha(r)\rangle = 0$ gives rise to

$$(m + \lambda/2\partial_r^2)\Gamma_a^{2d}|\Phi_\alpha(r)\rangle - i\lambda\partial_r\Gamma_b^{2d}|\Phi_\alpha(r)\rangle = 0. \quad (23)$$

Multiplying both sides by Γ_a^{2d} gives

$$(m + \lambda/2\partial_r^2)|\Phi_\alpha(r)\rangle = \lambda\partial_r C|\Phi_\alpha(r)\rangle. \quad (24)$$

Obviously, state $|\Phi_\alpha(r)\rangle$ should be the eigenstate of chiral operator C , namely $C|\Phi_z(r)\rangle = z|\Phi_z(r)\rangle$ with $z = \pm 1$. We set the trial wave function $|\Phi_z(r)\rangle = e^{\xi_z r}|\psi_z\rangle$, with $C|\psi_z\rangle = z|\psi_z\rangle$ and ξ_z is a complex number. By inserting this ansatz solution into Eq. (24), we have

$$\lambda_s/2\xi_{z_s}^2 - z_s\lambda_s\xi_s + m = 0. \quad (25)$$

The two roots are $\xi_z^{1,2} = \frac{z\lambda \pm \sqrt{\lambda^2 - 2m\lambda}}{\lambda}$. In the region $|t| < |\lambda|$, the real part of $\xi_z^{1,2}$ are negative and positive when $z = -1$ and $z = 1$, respectively. Under the boundary condition $|\Phi_z(0)\rangle = |\Phi_z(\infty)\rangle = 0$, we can know that the wave function of end states are $|\Phi_-(r)\rangle = \mathcal{N}(e^{\xi_-^1 r} - e^{\xi_-^2 r})|\psi_- \rangle$, with the normalization factor \mathcal{N} . On the contrast, if we consider the semi-system $r < 0$, then we will find that the end zero states should be the eigenstate of chiral operator C with eigenvalue $z = 1$. As a result, for a finite system with length L , the end zero states localized close to the end $r = 0$ and $r = L$ are the eigenstates of chiral operator C with eigenvalue $z = -1$ and $z = 1$, respectively. For $2^d \times 2^d$ matrix C , there are 2^{d-1} eigenstates with eigenvalue $z = 1$ and $z = -1$, respectively. Thus, there are 2^{d-1} end zero states localized at each end for $h(r)$. In the main text, we take $d = 2$ and $d = 3$, then there are two and four end zero states localized at each end, respectively. The spatial parts of the wave function for these end zero states are

$$f_-^s(r_s) = \mathcal{N}_s^-(e^{\xi_-^1 r_s} - e^{\xi_-^2 r_s}), f_+^s(r_s) = \mathcal{N}_s^+(e^{\xi_+^1(r_s-L_s)} - e^{\xi_+^2(r_s-L_s)}), \quad (26)$$

where $\mathcal{N}_s^-, \mathcal{N}_s^+$ are the normalization factors, index s denotes the different directions.

General principle of obtaining the CZESs

Considering arbitrary dD Bloch Hamiltonian

$$H(\mathbf{k}) = \sum_{s=1}^d h_s(k_s), \{C_s, h_s(k_s)\} = 0, \quad (27)$$

where $\mathbf{k} = (k_1, \dots, k_d)$, h_s belongs to the AIII symmetry class and respects the chiral symmetry C_s . Thus, 1D Hamiltonian h_s has a Z topological classification [63–65]. When h_s is topologically nontrivial characterized by the nonzero winding number, there are end zero states for this 1D system and their wave functions can be generically written as

$$|\Phi_{z_s}^s(r_s)\rangle = f_{z_s}^s(r_s)|\psi_{z_s}^s\rangle, C_s|\psi_{z_s}^s\rangle = z_s|\psi_{z_s}^s\rangle, \quad (28)$$

where spinor $|\psi_{z_s}^s\rangle$ is the eigenstate of C_s with eigenvalue $z_s = \pm 1$, scalar function $f_{z_s}^s(r_s)$ exponentially decays along r_s . Here, we have used the fact the end zero states always can be labeled by the eigenvalue of chiral symmetry C_s . Remarkably, when $|\psi_{z_1}^1\rangle = \dots = |\psi_{z_d}^d\rangle = |\psi_{(z_1, \dots, z_d)}\rangle$, we can construct the dD wave function

$$|\Psi_{z_1, \dots, z_d}(\mathbf{r})\rangle = \prod_{s=1}^d f_{z_s}^s(r_s)|\psi_{(z_1, \dots, z_d)}\rangle. \quad (29)$$

It is easy to see that

$$h_{s=1, \dots, d}|\Psi_{z_1, \dots, z_d}(\mathbf{r})\rangle = 0, H(-i\partial_{\mathbf{r}})|\Psi_{z_1, \dots, z_d}(\mathbf{r})\rangle = 0. \quad (30)$$

Thus, the state $|\Psi_{z_1, \dots, z_d}(\mathbf{r})\rangle$ is the zero energy state of Hamiltonian $H(-i\partial_{\mathbf{r}})$. Obviously, state $|\Psi_{z_1, \dots, z_d}(\mathbf{r})\rangle$ exponentially decays along all directions. Therefore, it is localized at the corner of a dD system and we obtain a CZESs.

Without loss of generality, we exemplify 1D Hamiltonian $h_s(k_s)$ with the form considered in Eq. (16). Explicitly, the considered Hamiltonian can be written as

$$H(\mathbf{k}) = \sum_{s=1}^d h_s(k_s), h_s(k_s) = M_s(k_s)\Gamma_{as}^{2d} + \lambda_s \sin k_s \Gamma_{bs}^{2d}. \quad (31)$$

Under the condition $|t_s| < |\lambda_s|$, we have shown that h_s is topologically nontrivial and the bulk topology is characterized by the winding numbers $\bar{\nu}_s = 2^{d-1}$. Taking the open boundary condition of k_s , h_s hosts 2^{d-1} end zero states localized at the ends $r_s = 0$ and $r_s = L_s$, respectively. The wave function of the end zero states can be written as $|\Phi_{z_s}^s(r_s)\rangle = f_{z_s}^s(r_s)|\psi_{z_s}^s\rangle$ with $C_s|\psi_{z_s}^s\rangle = z_s|\psi_{z_s}^s\rangle$.

When $2^d \times 2^d$ matrices $\{C_1, \dots, C_m, \dots, C_d\}$ commute with each other, they have 2^d common eigenstates labelled by their eigenvalue $(z_1, \dots, z_m, \dots, z_d)$. Correspondingly, we obtain 2^d CZESs with the wave function

$$|\Psi_{z_1, \dots, z_d}(\mathbf{r})\rangle = \prod_{s=1}^d f_{z_s}^s(r_s) |\psi_{(z_1, \dots, z_m, \dots, z_d)}\rangle, \quad (32)$$

with $C_m|\psi_{(z_1, \dots, z_m, \dots, z_d)}\rangle = z_m|\psi_{(z_1, \dots, z_m, \dots, z_d)}\rangle$. It can be readily verified that $h_{s=1,2,\dots,d}|\Psi_{z_1, \dots, z_d}(\mathbf{r})\rangle = 0$, giving rise to $H(-i\partial_{\mathbf{r}})|\Psi_{z_1, \dots, z_d}(\mathbf{r})\rangle = 0$. It is noted that the commutation relations between $\Gamma_{js}^{2^d}$ and $\Gamma_{j's'}^{2^d}$ have not been given still, with $s, s' \in \{1, \dots, d\}$, $j, j' = a, b$. However, these commutation relations will determine the topology property of $H(\mathbf{k})$ unambiguously. Under the condition $[C_s, C_{s'}] = 0$, 2D classification in the main text indicates there are four types commutation relations between $\Gamma_{js}^{2^d}$ and $\Gamma_{j's'}^{2^d}$, namely

$$\begin{aligned} \text{(i)} : & \{\Gamma_{as}^{2^d}, \Gamma_{as',bs'}^{2^d}\} = 0, \{\Gamma_{bs}^{2^d}, \Gamma_{as',bs'}^{2^d}\} = 0, \\ \text{(ii)} : & [\Gamma_{as}^{2^d}, \Gamma_{as',bs'}^{2^d}] = 0, [\Gamma_{bs}^{2^d}, \Gamma_{as',bs'}^{2^d}] = 0, \\ \text{(iii)} : & [\Gamma_{as}^{2^d}, \Gamma_{as',bs'}^{2^d}] = 0, \{\Gamma_{bs}^{2^d}, \Gamma_{as',bs'}^{2^d}\} = 0, \\ \text{(iv)} : & [\Gamma_{as}^{2^d}, \Gamma_{as'}^{2^d}] = 0, \{\Gamma_{as'}^{2^d}, \Gamma_{bs'}^{2^d}\} = 0, \\ & \{\Gamma_{as}^{2^d}, \Gamma_{bs'}^{2^d}\} = 0, [\Gamma_{as'}^{2^d}, \Gamma_{bs'}^{2^d}] = 0. \end{aligned} \quad (33)$$

Therefore, there are $4 \times 4^2 \times \dots \times 4^{d-1}$ types commutation relations for $H(\mathbf{k})$ when assign all the commutation relations between $\Gamma_{js}^{2^d}$ and $\Gamma_{j's'}^{2^d}$, with $s, s' \in \{1, \dots, d\}$, $j, j' = a, b$. Notably, here we do not distinguish the equivalent status between different directions. Once the commutation relations between all these Gamma matrices are given, we can predict a model featuring the CZESs in a arbitrary d D system. Remarkably, when the bulk and boundaries are gapped of the system, we will obtain a d th-order topological insulator.

The details and comparisons of different cases in 2D system

When $d = 2$ for the 2D Hamiltonian in Eq. (31), the Eq. 33 transform into the form

$$\begin{aligned} \text{(i)} : & \{\Gamma_{ax}^4, \Gamma_{ay,by}^4\} = 0, \{\Gamma_{bx}^4, \Gamma_{ay,by}^4\} = 0, \\ \text{(ii)} : & [\Gamma_{ax}^4, \Gamma_{ay,by}^4] = 0, [\Gamma_{bx}^4, \Gamma_{ay,by}^4] = 0, \\ \text{(iii)} : & [\Gamma_{ax}^4, \Gamma_{ay,by}^4] = 0, \{\Gamma_{bx}^4, \Gamma_{ay,by}^4\} = 0, \\ \text{(iv)} : & [\Gamma_{ax}^4, \Gamma_{ay}^4] = 0, \{\Gamma_{ay}^4, \Gamma_{by}^4\} = 0, \\ & \{\Gamma_{ax}^4, \Gamma_{by}^4\} = 0, [\Gamma_{ay}^4, \Gamma_{by}^4] = 0. \end{aligned} \quad (34)$$

Without loss of generality, we choose $\{\Gamma_x^a, \Gamma_x^b, C_x\} = \{\Gamma_1^4, \Gamma_2^4, \Gamma_{21}^4\}$. For the different commutation relations in Eq. 34, we can list all possible choices of $\{\Gamma_y^a, \Gamma_y^b, C_y\}$ as

$$\begin{aligned} \text{(i)} : & \{\Gamma_\alpha^4, \Gamma_\beta^4, \Gamma_{\beta\alpha}^4\}; \\ \text{(ii)} : & \{\Gamma_{\alpha\beta}^4, \Gamma_{\beta\gamma}^4, \Gamma_{\alpha\gamma}^4\}; \\ \text{(iii)} : & \{\Gamma_{2\alpha}^4, \Gamma_{2\beta}^4, \Gamma_{\beta\alpha}^4\}; \\ \text{(iv)} : & \{\Gamma_{2\alpha}^4, -\Gamma_{1\alpha}^4, \Gamma_{21}^4\}, \{\Gamma_1^4, \Gamma_2^4, \Gamma_{21}^4\}, \\ & \{\Gamma_{2\alpha}^4, \Gamma_2^4, -\Gamma_\alpha^4\}, \{\Gamma_1^4, \Gamma_{1\alpha}^4, \Gamma_\alpha^4\}; \end{aligned} \quad (35)$$

with $\alpha \neq \beta \neq \gamma \in (3, 4, 5)$. Thus, the situations $C_x \neq C_y$ and $C_x = C_y$ classified in the main text correspond to the cases (i-iv) and (iv), respectively.

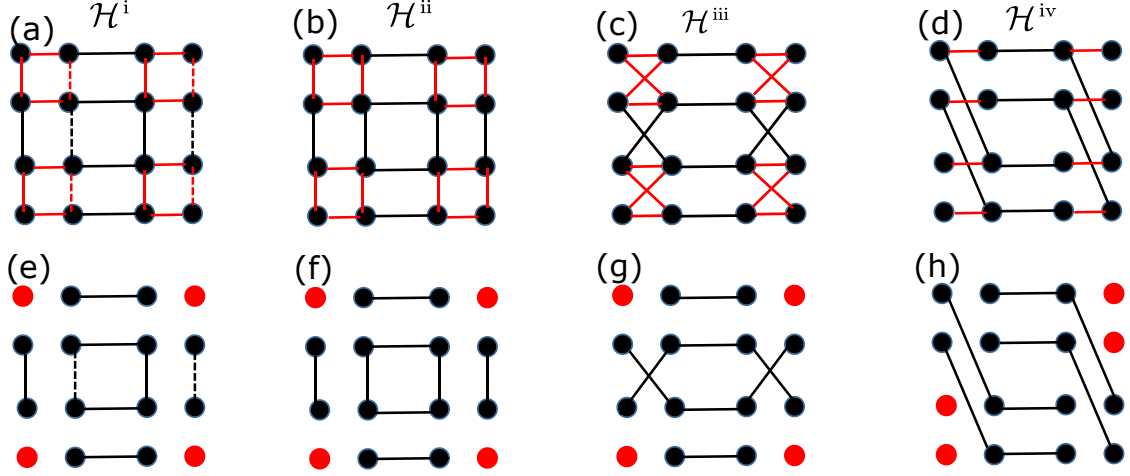


FIG. 4. (a)-(d) The schematic diagram of the lattice hoppings for Hamiltonians \mathcal{H}^{i-iv} . The red and black bonds represent the intracellular and intercellular hoppings, respectively. (e)-(h) Schematic of the lattice hoppings in the limit case $t_x = t_y = 0$ for Hamiltonians \mathcal{H}^{i-iv} . The existence of the CZESs corresponds to the presence of the isolated atoms at the corners in this limit case. For (e)-(g), the existence of isolated edge atoms coupled in a dimerized way corresponds to the existence of edge states described by the SSH model.

The 2D models predicted by the commutation relations (i-iii)

Making a classification for 2D Hamiltonian $H(\mathbf{k})$ ($d = 2$) in Eq.31, we can obtain four types commutation relations (i-iv) between the Gamma matrices, as discussed in the main text. For the case (i-iii), without loss of generality, we consider their representations as

$$\begin{aligned} \mathcal{H}^g(\mathbf{k}) &= h_x^g(k_x) + h_y^g(k_y), \\ h_x^i &= M_x(k_x)\tau_x\sigma_0 + \lambda_x \sin k_x \tau_y \sigma_0, h_y^i = M_y(k_y)\tau_z\sigma_x + \lambda_y \sin k_y \tau_z \sigma_y, \\ h_x^{ii} &= M_x(k_x)\tau_x\sigma_0 + \lambda_x \sin k_x \tau_y \sigma_0, h_y^{ii} = M_y(k_y)\tau_z\sigma_x + \lambda_y \sin k_y \tau_z \sigma_y, \\ h_x^{iii} &= M_x(k_x)\tau_x\sigma_0 + \lambda_x \sin k_x \tau_y \sigma_0, h_y^{iii} = M_y(k_y)\tau_x\sigma_x + \lambda_y \sin k_y \tau_x \sigma_y, \end{aligned} \quad (36)$$

with τ, σ two sets Pauli matrices and index $g = i, ii, iii$. It is noted that Hamiltonians $\mathcal{H}^i(\mathbf{k})$ and $\mathcal{H}^{ii}(\mathbf{k})$ have completely identical topology as the BBH and 2D SSH models and \mathcal{H}^{iii} denotes the crossed 2D SSH model. For Hamiltonians $\mathcal{H}^{i,ii,iii}(\mathbf{k})$, we have the chiral symmetries

$$\begin{aligned} C_x^i &= -\tau_z\sigma_0, C_y^i = -\tau_0\sigma_z, [C_x^i, C_y^i] = 0, C^i = C_x^i C_y^i = -\tau_z\sigma_z, \\ C_x^{ii} &= -\tau_z\sigma_0, C_y^{ii} = -\tau_0\sigma_z, [C_x^{ii}, C_y^{ii}] = 0, C^{ii} = C_x^{ii} C_y^{ii} = \tau_z\sigma_z, \\ C_x^{iii} &= -\tau_z\sigma_0, C_y^{iii} = -\tau_0\sigma_z, [C_x^{iii}, C_y^{iii}] = 0, C^{iii} = C_x^{iii} = -\tau_z\sigma_0. \end{aligned} \quad (37)$$

where $[C_s^g, h_s^g]_+ = 0, [C^g, \mathcal{H}^g]_+ = 0$, with indexs $s = x, y, g = i, ii, iii$. The hopping of these lattice models are schematically shown in Figs. 4(a)-(c). In Figs. 4(e)-(g), the presence of isolated atoms at the corners in the limit case $t_{x,y} = 0$ correspond to the existence of the CZESs.

Remarkably, the band structures of Hamiltonians $\mathcal{H}^{i,ii,iii}(\mathbf{k})$ can be clearly revealed by diagonalizing them in the σ space as

$$\begin{aligned} \mathcal{H}^i(\mathbf{k}) &= M_x(k_x)\tau_x\sigma_0 + \lambda_x \sin k_x \tau_y \sigma_0 + E_y \tau_z \sigma_\varphi, \\ \mathcal{H}^{ii}(\mathbf{k}) &= M_x(k_x)\tau_x\sigma_0 + \lambda_x \sin k_x \tau_y \sigma_0 + E_y \tau_0 \sigma_\varphi, \\ \mathcal{H}^{iii}(\mathbf{k}) &= M_x(k_x)\tau_x\sigma_0 + \lambda_x \sin k_x \tau_y \sigma_0 + E_y \tau_x \sigma_\varphi, \end{aligned} \quad (38)$$

where we have defined $E_y = \sqrt{M_y^2 + (\lambda_y \sin k_y)^2}$ and $\sigma_\varphi = \cos \varphi \sigma_x + \sin \varphi \sigma_y$, with $\tan \varphi = \lambda_y \sin k_y / M_y$. Thus, in

the eigenbasis of σ_φ , $\mathcal{H}^{i,ii,iii}$ are block-diagonal and two blocks Hamiltonians are

$$\begin{aligned} h_{\pm}^i(\mathbf{k}) &= M_x(k_x)\tau_x + \lambda_x \sin k_x \tau_y \pm E_y \tau_z, \\ h_{\pm}^{ii}(\mathbf{k}) &= M_x(k_x)\tau_x + \lambda_x \sin k_x \tau_y \pm E_y \tau_0, \\ h_{\pm}^{iii}(\mathbf{k}) &= (M_x(k_x) \pm E_y)\tau_x + \lambda_x \sin k_x \tau_y, \end{aligned} \quad (39)$$

with \pm the eigenvalues of σ_φ . With given k_y , $h_{\pm}^i, h_{\pm}^{ii}(\mathbf{k}), h_{\pm}^{iii}(\mathbf{k})$ can be viewed as the SSH model along k_x , with additional chiral symmetry breaking term $\pm E_y \tau_z$, modulated chemical potential term $\pm E_y \tau_0$, modulated intra-cell hopping term $\pm E_y \tau_x$, respectively. According to the Eq. (39), we know that the bulk energy spectrums of Hamiltonians $\mathcal{H}^{i-iii}(\mathbf{k})$ can be written as

$$\begin{aligned} E^i(\mathbf{k}) &= \pm \sqrt{E_x^2 + E_y^2}, E^{ii}(\mathbf{k}) = \pm E_x \pm E_y, \\ E^{iii}(\mathbf{k}) &= \pm \sqrt{(M_x \pm E_y)^2 + (\lambda_x \sin k_x)^2}, \end{aligned} \quad (40)$$

with $E_x = \sqrt{M_x^2 + (\lambda_x \sin k_x)^2}$, $E_y = \sqrt{M_y^2 + (\lambda_y \sin k_y)^2}$. Thus, for $\mathcal{H}^i(\mathbf{k})$, as long as $E_x \neq 0$ or $E_y \neq 0$, the bulk is full gapped. For $\mathcal{H}^{ii}(\mathbf{k})$, when $|E_x|_{\min} < |E_y|_{\max}$ or $|E_y|_{\min} < |E_x|_{\max}$, the bulk is fully gapped. Otherwise, the bulk is gapless and behave as a metal. For $\mathcal{H}^{iii}(\mathbf{k})$, when $||t_x| - |E_y||_{\min} > |\lambda_x|$, the bulk is fully gapped and behave as a trivial insulator or a 2th-order TI when $|t_{x,y}| < |\lambda_{x,y}|$. When $|t_x| + |E_y|_{\max} < |\lambda_x|$, or $||t_x| - |E_y||_{\max} < |\lambda_x|$ and $|t_x| + |E_y|_{\min} > |\lambda_x|$, the bulk is fully gapped and behave as a weak topological insulator characterized by the edge flat bands, as shown in Figs. 5(a)(b). Otherwise, the bulk is gapless and behave as mirror symmetry protected Weyl semimetal characterized by edge flat bands, as shown in Figs. 5(c)-(f).

When the bulk is fully gapped, the occupied states for Hamiltonians $\mathcal{H}^{i-iii}(\mathbf{k})$ can be written as

$$\begin{aligned} |\Psi_1^i\rangle &= (\sin \theta/2, -\cos \theta/2 e^{i\phi})^T \otimes (1, e^{i\varphi})^T / \sqrt{2}, \\ |\Psi_2^i\rangle &= (\cos \theta/2, -\sin \theta/2 e^{i\phi})^T \otimes (1, -e^{i\varphi})^T / \sqrt{2}, \\ |\Psi_1^{ii}\rangle &= (1, e^{i\phi})^T \otimes (1, -e^{i\varphi})^T / 2, |\Psi_2^{ii}\rangle = (1, -e^{i\phi})^T \otimes (1, -e^{i\varphi})^T / 2, \\ |\Psi_1^{iii}\rangle &= (1, -e^{i\beta_1})^T \otimes (1, e^{i\varphi})^T / 2, |\Psi_2^{iii}\rangle = (1, -e^{i\beta_2})^T \otimes (1, -e^{i\varphi})^T / 2, \end{aligned} \quad (41)$$

with $\cos \theta = E_y/|E^i|$, $\tan \phi = \lambda_x \sin k_x / M_x$, $\tan \beta_1 = \lambda_x \sin k_x / (M_x + E_y)$, $\tan \beta_2 = \lambda_x \sin k_x / (M_x - E_y)$. Here, for the definition of the occupied states, we consider the parameters region $|E_x|_{\min} < |E_y|_{\max}$ for $\mathcal{H}^{ii}(\mathbf{k})$.

The comparisons of the topological characterizations

In the following, we compare the different topological characterizations, including nested Wilson loop, polarization, quadrupole moment, and edge winding number, for the second-order TI phase in cases (i-iii). It is known that the CZESs in the BBH model can be characterized by the nested Wilson loop topological invariants, which reflect the topology of the gapped Wannier band. From the bulk wave function in Eq. (41), the Wannier bands $\nu(k_y)$, the momentum dependent Berry phase of the occupied states, can be calculated as

$$\nu_n^g(k_y) = \int_{-\pi}^{\pi} A_n^g(\mathbf{k}) dk_x = -i \int_{-\pi}^{\pi} \langle \Psi_n^g(\mathbf{k}) | \partial_{k_x} | \Psi_n^g(\mathbf{k}) \rangle dk_x, \quad (42)$$

with the occupied states index $n = 1, 2$, $A_n^g(\mathbf{k})$ the Berry connection. According to the Eq. (41), we have

$$\begin{aligned} A_1^i &= \cos^2 \theta / 2 \partial_{k_x} \phi, A_2^i = \sin^2 \theta / 2 \partial_{k_x} \phi, \\ A_1^{ii} &= A_2^{ii} = \partial_{k_x} \phi / 2, A_1^{iii} = \partial_{k_x} \beta_1 / 2, A_2^{iii} = \partial_{k_x} \beta_2 / 2. \end{aligned} \quad (43)$$

After the integration for the Berry connection, the Wannier bands $\nu_1^i(k_y) = 2\pi \cos^2 \theta / 2$, $\nu_2^i(k_y) = 2\pi \sin^2 \theta / 2$. Thus, the Wannier bands $\nu_{1,2}^i$ for $\mathcal{H}^i(\mathbf{k})$ are gapped when $E_y \neq 0$. Otherwise when $E_y = 0$, the chiral symmetry for h_{\pm}^i restores and the Wannier bands are gapless at $k_y = 0/\pi$, namely $\nu_1^i(k_y = 0/\pi) = \nu_2^i(k_y = 0/\pi)$. Thus, the Wannier band $\nu_n^i(k_y)$ has the same topological phase transition condition as h_y . Analogously, Wannier band $\nu_n^i(k_x)$ has the same topological phase transition condition as h_x . Thus, the CZESs existing condition $\nu_{x,y} = 1$ can be extracted from the Wannier band topology through the nested Wilson loop topological invariants. Nevertheless, because ϕ, β_1, β_2 are the periodic function of k_x , the Berry phases $\nu_n^{ii,iii}(k_y)$ for the occupied states of $\mathcal{H}^{ii,iii}(\mathbf{k})$ are always quantized to 0 or π , which indicates that the Wannier bands are gapless for these two cases. Then the nested Wilson loop method

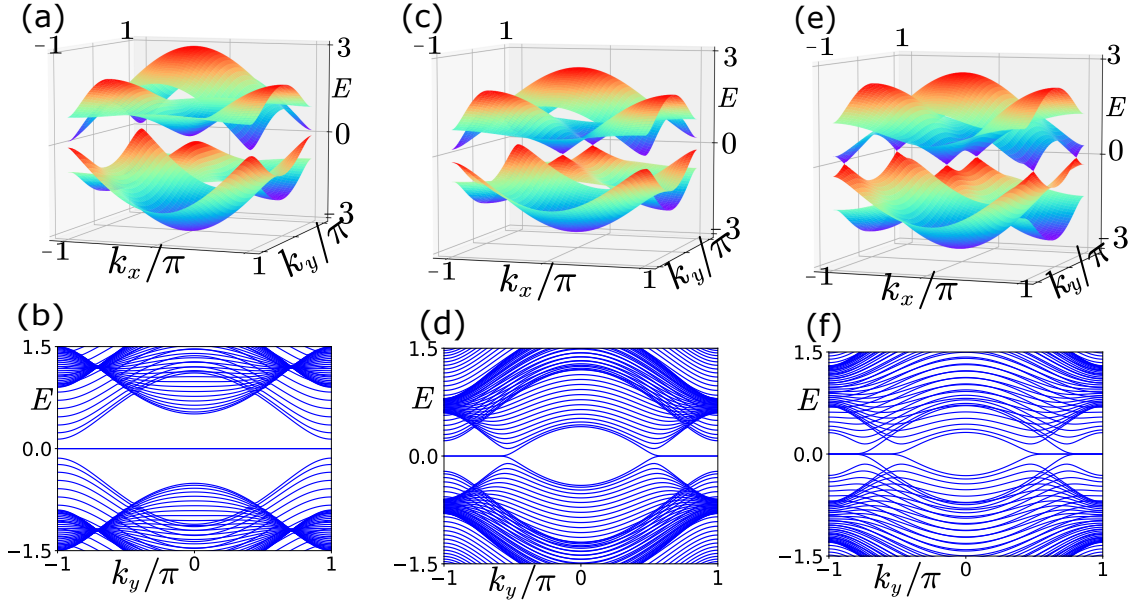


FIG. 5. (a)(b) The bulk energy spectrum and edge flat bands of the weak TI phase are plotted. We take the parameters as $\lambda_x = 1, t_x = 0.6, \lambda_y = 1, t_y = 0.5$. (c)(d) The bulk energy spectrum and edge flat bands of the Weyl semimetal with two Weyl points are plotted. We take the parameters as $\lambda_x = 1, t_x = 0.6, \lambda_y = 0.7, t_y = 0.4$. (e)(f) The bulk energy spectrum and edge flat bands of the Weyl semimetal with two Weyl points are plotted. We take the parameters as $\lambda_x = 1, t_x = 0.6, \lambda_y = 1, t_y = 0.2$.

fails to characterize the CZESs in cases (ii,iii). Thus, the nested Wilson loop characterizations for the CZE are only valid for case (i).

For the 2D SSH model, it has been shown that the CZE can be characterized by the bulk polarization. For example, the polarization along x direction can be written as

$$\begin{aligned} P_x^g &= \frac{i}{4\pi^2} \sum_n \int dk_y dk_x \text{Tr}[\langle \Psi_n^g(\mathbf{k}) | \partial_{k_x} | \Psi_n^g(\mathbf{k}) \rangle] \\ &= \frac{1}{4\pi^2} \int dk_y (\nu_1^g(k_y) + \nu_2^g(k_y)). \end{aligned} \quad (44)$$

For model $\mathcal{H}^i(\mathbf{k})$, because the chiral symmetry breaking term $E_y \tau_z$ is opposite for h_+ and h_- , we have $\nu_1^i(k_y) + \nu_2^i(k_y) = 2\pi$, giving rise to trivial polarization. Thus, the polarization characterization for the CZE is invalid for this case. For model $\mathcal{H}^{ii}(\mathbf{k})$, $\nu_{1,2}^{ii}(k_y)$ are both quantized to π and 0 when $\nu_x = 1$ and $\nu_x = 0$, respectively. The former case leads to nontrivial polarization for each band. Similarly, $\nu_{1,2}^{ii}(k_x)$ are both quantized to π and 0 when $\nu_y = 1$ and $\nu_y = 0$, respectively. Thus the CZE can be characterized by the polarization of each band for this case. For the second-order TI phase in model $\mathcal{H}^{iii}(\mathbf{k})$, the Berry phase $\nu_{1,2}^{iii}(k_y)$ are both quantized to the value 0, leading to trivial polarization. Thus, the polarization topological invariant also can not characterize the existence of the CZE for this case.

It is known that quadrupole moment as a higher-order topological invariant can characterize the existence CZE in the BBH model [57, 58]. The quadrupole moment can be calculated in real space and it is given by

$$Q_{xy} = [\frac{1}{2\pi} \text{Imlog}[\det(U^\dagger \hat{Q} U)] - q_{xy}] \text{mod} 1 \quad (45)$$

where the matrix U is constructed by column-wise packing of the occupied eigenstates under the periodic boundary conditions, $\hat{Q} = e^{2\pi i \hat{x} \hat{y} / L_x L_y}$ and \hat{x}, \hat{y} are the position operators, $q_{xy} = \frac{1}{2} \sum_{j=1}^n x_j y_j / (L_x L_y)$ is the contribution from the background positive charge distribution, with n the dimension of the bulk Hamiltonian. Our numerical calculations show that the quadrupole moment topological invariant Q_{xy} can characterize the CZE for Hamiltonian $\mathcal{H}^{iii}(\mathbf{k})$, but can not characterize the CZE for Hamiltonian $\mathcal{H}^{ii}(\mathbf{k})$. The numerical results are shown in Figs. 6(b)(c). Moreover distinct from the BBH model where $p_x^{\text{edge}} = p_y^{\text{edge}} = 0.5$, the edge polarizations $p_x^{\text{edge}} = 0.5, p_y^{\text{edge}} = 0.$, as shown in Figs. 6(e)(f) in model $\mathcal{H}^{iii}(\mathbf{k})$. Thus, the second-order TI phase in $\mathcal{H}^{iii}(\mathbf{k})$ is a phase of type-II quadrupole TI.

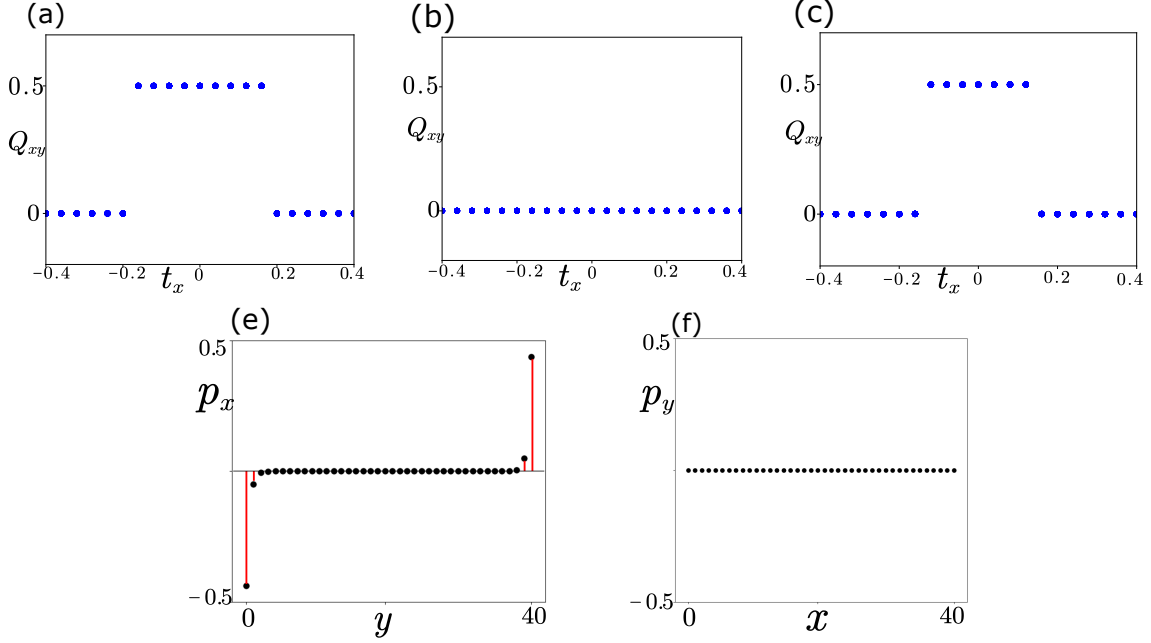


FIG. 6. (a)-(c) The quadrupole moment numerical calculations for the fully gapped phases in cases (i-iii). Common parameters are taken as $\lambda_x = 0.2, \lambda_y = 1, t_y = 0.3$. We perform the numerical calculation with the size 41×41 . It is noted that the small deviation from the exact phase transition point $|t_x| = 0.2$ in (c) is resulted by the size effect. (e)(f) The numerical calculations of edge polarizations ($p_x^{\text{edge}}, p_y^{\text{edge}}$) for the case (iii). We take the parameters as $t_x = 0.1, \lambda_x = 0.2, t_y = 0.3, \lambda_y = 1$.

In the main text, we have shown that the edge winding number $\tilde{\nu}_x = 1$ can completely reflect the CZE's existing condition $\nu_{x,y} = 1$. For the BBH and 2D SSH models, there are edge states along k_x and k_y directions, as shown in Figs.7(a)(b) and (c)(d), respectively. Generally, the wave function of the edge states along k_x and k_y can be written as

$$\begin{aligned} |\Psi^g(k_x, r_y)\rangle_{z_y} &= f_{z_y}^g(r_y) P_{z_y}^g |\psi^g(k_x)\rangle, h_x^g(k_x) |\psi^g(k_x)\rangle = E_x(k_x) |\psi^g(k_x)\rangle, \\ |\Psi^g(r_x, k_y)\rangle_{z_x} &= f_{z_x}^g(r_x) P_{z_x}^g |\psi^g(k_y)\rangle, h_y^g(k_y) |\psi^g(k_y)\rangle = E_y(k_y) |\psi^g(k_y)\rangle, \end{aligned} \quad (46)$$

with the projection operators $P_{z_x}^g = (1 + z_x C_x^g)/2$ and $P_{z_y}^g = (1 + z_y C_y^g)/2$, $g=i,ii$. It can be readily verified that

$$\begin{aligned} \mathcal{H}(k_x, r_y) |\Psi^g(k_x, r_y)\rangle_{z_y} &= E_x(k_x) |\Psi^g(k_x, r_y)\rangle_{z_y}, \\ \mathcal{H}(r_x, k_y) |\Psi^g(r_x, k_y)\rangle_{z_x} &= E_y(k_y) |\Psi^g(r_x, k_y)\rangle_{z_x}, \end{aligned} \quad (47)$$

which means that the edge states $|\Psi^g(k_x, r_y)\rangle_{z_y}$ and $|\Psi^g(r_x, k_y)\rangle_{z_x}$ have the same energy spectrum as h_x and h_y , respectively. Notably, the existence of the edge states along k_x and k_y requires $[C_y^g, h_x^g] = 0$ and $[C_x^g, h_y^g] = 0$, respectively. Otherwise, $|\Psi^g(k_x, r_y)\rangle_{z_y}$ or $|\Psi^g(r_x, k_y)\rangle_{z_x}$ is a null vector after the projection. It can be readily verified that $[C_x^{i,ii}, h_y] = 0, [C_y^{i,ii}, h_x] = 0$ for both cases (i) and (ii), and $\{C_x^{iii}, h_y\} = 0, [C_y^{iii}, h_x] = 0$ for case (iii). Thus, there are both edge states along k_x and k_y for cases (i-ii), but there are edge states only along k_x for case (iii), as shown in Figs. 7(e)(f). Correspondingly, the edge Hamiltonian describing these edge states can be obtained by projecting h_x or h_y into the subspace defined by P_{z_y} or P_{z_x} . Then we will find that these edge states are described by a SSH model, which consists with the existence of edge isolated atoms coupled in a dimerized way in the limit case $t_x = t_y = 0$, as shown in Figs. 4(e)-(g). Remarkably, the existence of edge states along k_x and k_y require that h_y and h_x are topologically nontrivial, respectively. Thus, the edge winding number $\tilde{\nu}_x = 1$ or $\tilde{\nu}_y = 1$ of the 1D edge states can completely reflect the CZE's existing conditions $\nu_x = \nu_y = 1$. As a result, the edge winding number can completely characterize the existence of the CZE's for cases (i-iii), revealing the unified edge-corner correspondence.

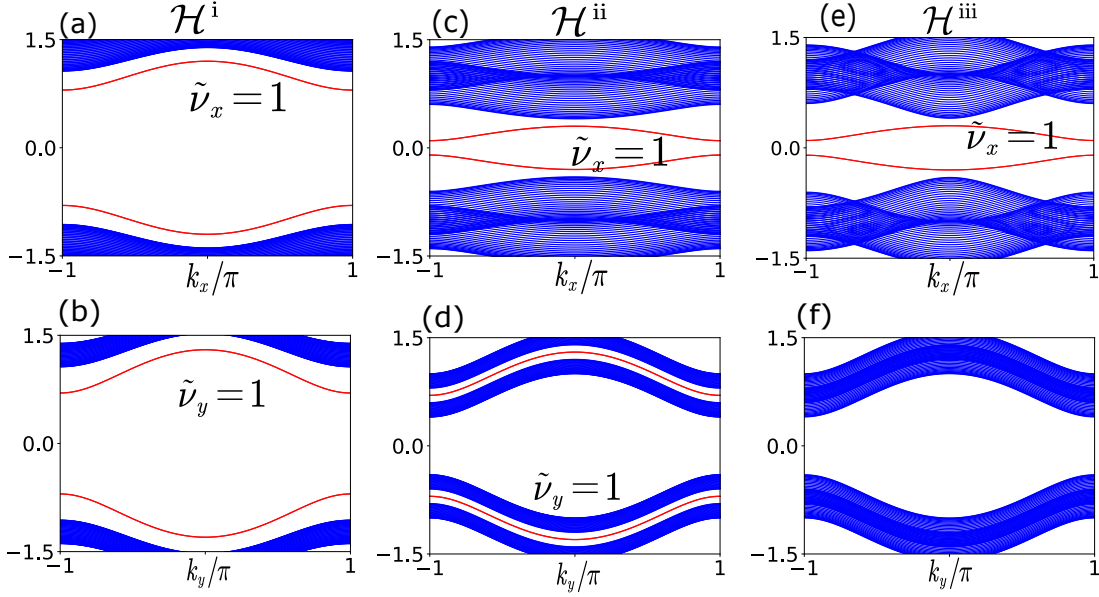


FIG. 7. (a)(b) The energy spectrum for $\mathcal{H}^i(\mathbf{k})$ with ribbon geometry along k_x and k_y directions, respectively. We take model parameters as $\lambda_x = \lambda_y = 1, t_x = 0.2, t_y = 0.3$. (c)(d) The energy spectrum for $\mathcal{H}^{ii}(\mathbf{k})$ with ribbon geometry along k_x and k_y directions, respectively. We take model parameters as $\lambda_x = 0.2, \lambda_y = 1, t_x = 0.1, t_y = 0.3$. (e)(f) The energy spectrum for $\mathcal{H}^{iii}(\mathbf{k})$ with ribbon geometry along k_x and k_y directions, respectively. We take model parameters as $\lambda_x = 0.2, \lambda_y = 1, t_x = 0.1, t_y = 0.3$.

The model predicted by the commutation relation (iv)

In the main text, classifying the 2D system constructed by the SSH model from each direction, we obtain the case (iv) and it can be realized by considering the Hamiltonian

$$\begin{aligned} \mathcal{H}^{iv}(\mathbf{k}) &= M_x(k_x)\Gamma_x^a + \lambda_x \sin k_x \Gamma_x^b + \lambda_y M_y(k_y)\Gamma_y^a + \sin k_y \Gamma_y^b, \\ \Gamma_x^a &= \tau_z \sigma_x, \Gamma_x^b = \tau_z \sigma_y, \Gamma_y^a = \tau_0 \sigma_x, \Gamma_y^b = \tau_0 \sigma_y. \end{aligned} \quad (48)$$

The lattice hopping of $\mathcal{H}^{iv}(\mathbf{k})$ is shown in Figs. 4(d)(h). For this concrete model, we have chiral symmetries $C_x^{iv} = C_y^{iv} = -\sigma_z$ and $\Gamma_x^a \Gamma_y^a = \tau_z \sigma_0$, which commutes with Hamiltonian $\mathcal{H}^{iv}(\mathbf{k})$. Correspondingly, \mathcal{H}^{iv} is block diagonal in τ space and each block can be written as $h_{\pm}^{iv} = (\pm M_x + M_y)\sigma_x + (\pm \lambda_x \sin k_x + \lambda_y \sin k_y)\sigma_y$. Here, h_+ and h_- have the identical physics and we focus on the block h_+^{iv} . This two bands model can be separated into two 1D Hamiltonians $h'_{s=x,y} = (t'_s + \lambda_s \cos k_s)\sigma_x + \lambda_s \sin k_s \sigma_y$ with $t'_x + t'_y = t_x + t_y = t$. As long as h'_x and h'_y are topologically nontrivial with end zero states, the 2D Hamiltonian h_+ has CZE localized at the diagonal corners according to our construction principle. Thus, there are CZE for h_+ when $|t| < |\lambda_x| + |\lambda_y|$.

Obviously, h_+^{iv} can be viewed as a modulated SSH along $k_{x/y}$, with $k_{y/x}$ given. The band structures can be clearly revealed by the Berry phase $\nu^{iv}(k_x)$ or $\nu^{iv}(k_y)$ of the occupied state of h_+ , with k_x or k_y given. When $\nu^{iv}(k_x)$ or $\nu^{iv}(k_y)$ is quantized to π over all the range, the bulk behave as a weak TI characterized by edge flat band, corresponding to the condition $|t| + |\lambda_x| < |\lambda_y|$ or $|t| + |\lambda_y| < |\lambda_x|$. When $\nu^{iv}(k_y)$ and $\nu^{iv}(k_x)$ are both quantized to 0 over all the range, corresponding to the condition $|t| > |\lambda_x| + |\lambda_y|$, the bulk is a normal insulator. When $\nu^{iv}(k_x)$ or $\nu^{iv}(k_y)$ is not successive, corresponding to the condition $||t| - |\lambda_x|| < |\lambda_y| < |t| + |\lambda_x|$ or $||t| - |\lambda_y|| < |\lambda_x| < |t| + |\lambda_y|$, the bulk is a Weyl semimetal characterized by edge flat band. Thus, distinct from the case (iii), the predicted CZE here always coexist with the edge flat band, which brings the difficulty to identify and characterize the predicted CZE.

The CZE in the superconducting system

In the main text, we consider the 2D electronic system constructed by the combination of the SSH model along different directions. By classifying this system, we obtain four topologically unequivalent models supporting the CZE. In the following, we show that all these models with different commutation relations between the Gamma matrices

can be realized in the superconducting system by allowing additional particle-hole symmetry. Directly, considering in the superconducting Bogoliubov-de Gennes (BdG) basis $\Psi(\mathbf{k}) = (c_{\uparrow,\mathbf{k}}, c_{\downarrow,\mathbf{k}}, c_{\uparrow,\mathbf{k}}^\dagger, c_{\downarrow,\mathbf{k}}^\dagger)$, the BDG Hamiltonian can be generically written as

$$H_{\text{BDG}}(\mathbf{k}) = M_e(\mathbf{k})(\tau_z s_0 + \tau_z s_x + \tau_z s_z + \tau_0 s_y) + M_o(\mathbf{k})(\tau_0 s_x + \tau_0 s_z + \tau_z s_y) + \Delta_e(\mathbf{k})(\tau_y s_y + \tau_x s_y) + \Delta_o(\mathbf{k})(\tau_x s_0 + \tau_x s_z + \tau_x s_x + \tau_y s_0 + \tau_y s_x + \tau_y s_z), \quad (49)$$

where, τ, s are Pauli matrices in the particle-hole and spin space, respectively. Here, required by the particle-hole symmetry $\mathcal{P} = \tau_x K$, we have $M_e(\mathbf{k}) = M_e(-\mathbf{k})$, $M_o(\mathbf{k}) = -M_o(-\mathbf{k})$, $\Delta_e(\mathbf{k}) = \Delta_e(-\mathbf{k})$, $\Delta_o(\mathbf{k}) = -\Delta_o(-\mathbf{k})$. Obviously, all the 15 traceless Dirac matrices can enter into the BDG Hamiltonian. In the following, we consider the BDG Hamiltonian

$$\mathcal{H}_{\text{BDG}} = M_x(k_x)\Gamma_x^a + \lambda_x \sin k_x \Gamma_x^b + \lambda_y M_y(k_y)\Gamma_y^a + \sin k_y \Gamma_y^b, \quad (50)$$

with

$$\begin{aligned} \Gamma_x^a, \Gamma_y^a &\in \{\tau_z s_0, \tau_z s_x, \tau_z s_z, \tau_0 s_y, \tau_y s_y, \tau_x s_y\}, \\ \Gamma_x^b, \Gamma_y^b &\in \{\tau_0 s_x, \tau_0 s_z, \tau_z s_y, \tau_x s_0, \tau_x s_z, \tau_x s_x, \tau_y s_0, \tau_y s_x, \tau_y s_z\}. \end{aligned} \quad (51)$$

Under the CZE's existing condition $[i\Gamma_x^a \Gamma_y^b, i\Gamma_y^a \Gamma_x^b] = 0$ for the BDG Hamiltonian \mathcal{H}_{BDG} , we will show that all four types commutation relations between the Dirac matrices can be realized.

For the case (i), we require $\{\Gamma_x^a, \Gamma_y^{a,b}\} = 0, \{\Gamma_x^b, \Gamma_y^{a,b}\} = 0$. This case can be realized by considering the representations

$$\begin{aligned} \mathcal{H}_{\text{BDG1}}^i(\mathbf{k}) &= M_x(k_x)\tau_z s_x + \lambda_x \sin k_x \tau_y s_x + \lambda_y M_y(k_y)\tau_0 s_y + \sin k_y \tau_x s_x, \\ \mathcal{H}_{\text{BDG2}}^i(\mathbf{k}) &= M_x(k_x)\tau_z s_x + \lambda_x \sin k_x \tau_x s_0 + \lambda_y M_y(k_y)\tau_z s_z + \sin k_y \tau_y s_0, \\ \mathcal{H}_{\text{BDG3}}^i(\mathbf{k}) &= M_x(k_x)\tau_y s_y + \lambda_x \sin k_x \tau_0 s_x + \lambda_y M_y(k_y)\tau_x s_y + \sin k_y \tau_z s_y, \\ \mathcal{H}_{\text{BDG4}}^i(\mathbf{k}) &= M_x(k_x)\tau_z s_0 + \lambda_x \sin k_x \tau_x s_z + \lambda_y M_y(k_y)\tau_x s_y + \sin k_y \tau_y s_0, \\ \mathcal{H}_{\text{BDG5}}^i(\mathbf{k}) &= M_x(k_x)\tau_z s_0 + \lambda_x \sin k_x \tau_x s_0 + \lambda_y M_y(k_y)\tau_y s_y + \sin k_y \tau_y s_x, \\ \mathcal{H}_{\text{BDG6}}^i(\mathbf{k}) &= M_x(k_x)\tau_z s_z + \lambda_x \sin k_x \tau_0 s_x + \lambda_y M_y(k_y)\tau_0 s_y + \sin k_y \tau_x s_z. \end{aligned} \quad (52)$$

The bulk states of these Hamiltonians are fully gapped and they behave as the second-order TSCs, which have completely identical topology property as the BBH model. It is noted that the models $\mathcal{H}_{\text{BDG1}}^i(\mathbf{k})$ and $\mathcal{H}_{\text{BDG2}}^i(\mathbf{k})$ have been studied in references [81, 82]. The realization of the model $\mathcal{H}_{\text{BDG3}}^i(\mathbf{k})$ only need the even parity pairings, breaking or preserving time-reversal symmetry ($\mathcal{T} = i s_y K$), which has been considered in reference [37]. Besides the model Hamiltonian $\mathcal{H}_{\text{BDG3}}^i(\mathbf{k})$, the realizations of other model Hamiltonians require the p -wave pairings, breaking or preserving time-reversal symmetry.

For the case (ii), we require $[\Gamma_x^a, \Gamma_y^{a,b}] = 0, [\Gamma_x^b, \Gamma_y^{a,b}] = 0$. This case can be realized by considering the representation

$$\mathcal{H}_{\text{BDG1}}^{\text{ii}}(\mathbf{k}) = M_1(k_1)\tau_z s_0 + \sin k_1 \tau_x s_x + M_2(k_2)\tau_z s_z + \sin k_2 \tau_0 s_x. \quad (53)$$

The realization of this concrete model requires the p -wave pairing for the system.

For the case (iii), we require $[\Gamma_x^a, \Gamma_y^{a,b}] = 0, \{\Gamma_x^b, \Gamma_y^{a,b}\} = 0$. This case can be realized by considering the representation

$$\begin{aligned} \mathcal{H}_{\text{BDG1}}^{\text{iii}}(\mathbf{k}) &= M_1(k_1)\tau_z s_x + \sin k_1 \tau_y s_0 + M_2(k_2)\tau_z s_0 + \sin k_2 \tau_x s_z, \\ \mathcal{H}_{\text{BDG2}}^{\text{iii}}(\mathbf{k}) &= M_2(k_2)\tau_z s_x + \sin k_2 \tau_z s_y + M_1(k_1)\tau_y s_y + \sin k_1 \tau_0 s_x. \end{aligned} \quad (54)$$

The realization of model Hamiltonian $\mathcal{H}_{\text{BDG1}}^{\text{iii}}(\mathbf{k})$ needs the p -wave pairing. The realization of model Hamiltonian $\mathcal{H}_{\text{BDG2}}^{\text{iii}}(\mathbf{k})$ only needs the even parity pairing preserving time-reversal symmetry.

For the case (iv), we require $[\Gamma_x^a, \Gamma_y^a] = 0, \{\Gamma_x^b, \Gamma_y^b\} = 0, \{\Gamma_x^a, \Gamma_y^b\} = 0, [\Gamma_x^b, \Gamma_y^b] = 0$. This case can be realized by considering the representation

$$\mathcal{H}_{\text{BDG}}^{\text{iv}}(\mathbf{k}) = M_1(k_1)\tau_z s_0 + \sin k_1 \tau_x s_z + M_2(k_2)\tau_z s_0 + \sin k_2 \tau_y s_x. \quad (55)$$

The realization of model Hamiltonian $\mathcal{H}_{\text{BDG}}^{\text{iv}}(\mathbf{k})$ needs the p -wave pairing.